Astronomy & Astrophysics manuscript no.
(will be inserted by hand later)

The strange case of the massive binary HD 149404*

G. Rauw[1** ‡], Y. Nazé[1***], F. Carrier[2], G. Burki[2], E. Gosset[1 † ‡], and J.-M. Vreux[1]

[1] Institut d'Astrophysique et de Géophysique, Université de Liège, 5, Avenue de Cointe, B-4000 Liège, Belgium
[2] Observatoire de Genève, CH-1290 Sauverny, Switzerland

Received date / Accepted date

Abstract. We report the analysis of an extensive set of high-resolution spectroscopic observations of the massive binary system HD 149404. We compare different techniques to measure the radial velocities of the heavily blended absorption lines and we derive a new orbital solution. The absorption lines display strong variability that slightly affects the orbital solution and the determination of the spectral types of the components of the binary. We find that the primary is probably of spectral type O7.5 I(f), while the secondary is most likely an ON9.7 I supergiant.
The secondary seems to be the most evolved component of the system and its current evolutionary status could best be explained if the system has undergone a Roche lobe overflow episode during the past. The secondary could actually still be rather close to filling its critical volume and this could lead to an enhanced mass loss of the secondary.
The spectrum of HD 149404 displays many emission lines some of which show phase-locked line profile variations. In particular, the Hα line displays a double-peaked morphology at orbital phases near conjunction. We investigate the radial velocity behaviour of the emission lines and we find that some of them must be formed in an interaction region. We propose a simple model where some of the optical emission lines arise in a heavily bended shock region.

Key words. stars: early-type – binaries: spectroscopic – stars: individual: HD 149404

1. Introduction

Over the last decade, substantial progress has been achieved in our understanding of the interaction processes in early-type binary systems. It has been shown that some of the emission lines in the spectra of O-star binaries are at least partially formed in the wind interaction region (e.g. Thaller 1997). Observations of the phase-locked emission line profile variability can be used to constrain the geometry of the interaction region and allow us in principle to distinguish between a colliding wind phenomenon and a Roche lobe overflow (RLOF) process (e.g. Wiggs & Gies 1993, Rauw et al. 1999). A detailed analysis of the interaction phenomena in binaries in different evolutionary stages is therefore crucial for our understanding of stellar evolution as well as for a determination of the properties of the stellar winds of the binary components.

In the present paper, we discuss an extensive set of spectra of HD 149404 (= HR 6164 = V 918 Sco). Walborn (1972) assigned an O9 Ia spectral type to the global spectrum of this system. Later on, it was discovered that some lines were actually double, but heavily blended (Conti et al. 1977). A first orbital solution was derived by Massey & Conti (1979) from a set of optical spectra, and another one was obtained by Stickland & Koch (1996) from *IUE* observations (see Table 4). Several spectral features of HD 149404 point towards an interaction between the two components. In fact, Massey & Conti (1979) noticed the double-peaked structure of the Hα emission profile in the spectrum of HD 149404 and they interpreted this feature as a signature of an ongoing Roche lobe overflow process. More recently, Thaller (1998) suggested that the behaviour of the two Hα peaks was due to a colliding wind interaction. HD 149404 is also known to display the so-called 'Struve-Sahade effect' (Stickland 1997). So far, the origin of this effect remains unclear although Gies et al. (1997) suggest that it could result from photospheric heating by the X-ray emission generated in the wind interaction region.

This paper is organized as follows: the observations and the data reduction are presented in Sect. 2 and the spectral features of HD 149404 are discussed in Sect. 3. Different techniques are used to measure the radial velocities of the absorp-

Send offprint requests to: G. Rauw

* Based on observations collected at the European Southern Observatory (La Silla, Chile) and at the Cerro Tololo Inter-American Observatory (CTIO).
** Postdoctoral Researcher FNRS (Belgium)
*** Research Fellow FNRS (Belgium)
† Research Associate FNRS (Belgium)
‡ Visiting Astronomer, CTIO, National Optical Astronomy Observatories (NOAO). NOAO is operated by the Association of Universities for Research in Astronomy, Inc. under contract with the National Science Foundation.

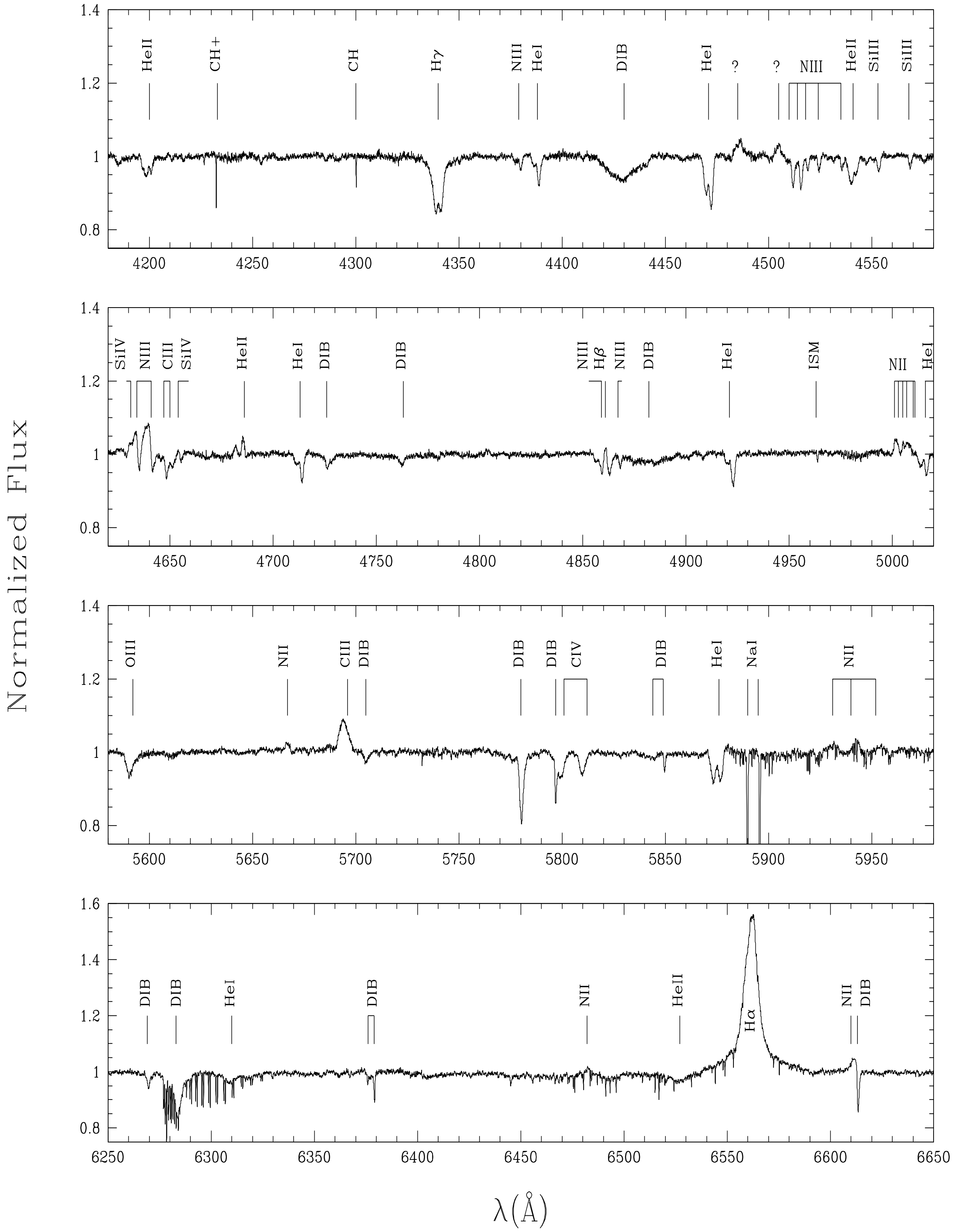

Fig. 1. Spectrum of HD 149404 as observed with the FEROS spectrograph on HJD 2451299.800 ($\phi = 0.23$). At this orbital phase, the spectrum of the most massive star is shifted towards the blue.

tion lines and a new orbital solution is derived in Sect. 4. In Sect. 5, we discuss the luminosity ratio of the binary components. As a next step, we examine the variations of the emission lines (Sect. 6). Finally, we discuss a possible model for the interaction in HD 149404 as well as the evolutionary status of the system (Sect. 7).

2. Observations and data reduction

We observed HD 149404 over a period of 3 years with various instruments. A first set of spectra, covering roughly 45 Å centred on the He I λ 4471, He II λ 4686 and N III $\lambda\lambda$ 4634-41 lines, was obtained in June 1997 with the 1.4 m Coudé Auxiliary Telescope (CAT) at ESO, La Silla, feeding the Coudé Echelle Spectrometer (CES) and the Long Camera (LC). Additional data (covering 20 Å around the He I λ 4471 and He II λ 4686 lines) were taken with the same spectrograph equipped with the Very Long Camera (VLC) in April-May 1998 and July 1998. In all cases, the detector was ESO CCD#38, a Loral 2688×512 CCD with pixel size 15 μm × 15 μm. The nominal resolving power was 70 000 - 80 000. Typical exposure times were of the order of 15 minutes and the average signal-to-noise ratio was about 150.

In May 1999 and May 2000, we observed HD 149404 with the Fiber-fed Extended Range Optical Spectrograph (FEROS, Kaufer et al. 1999) at the ESO 1.52 m telescope at La Silla. The spectra cover the wavelength range 3650 - 9200 Å with a resolving power of 48 000. The detector was a 2k × 4k EEV CCD with pixel size 15 μm × 15 μm. The typical exposure time was 2 minutes and the S/N ratio at 6000 Å is about 160.

Five more spectra were taken in May-June 1999 with the Bench-Mounted Echelle spectrograph (BME) fed by the 1.5 m Ritchey-Chrétien telescope at CTIO. These data covered the spectral range 3750 - 5800 Å. The typical S/N ratio was 120 at 4620 Å for exposure times of about 20 minutes. The detector used was a TEK CCD with 2048 × 2048 pixels of 24 μm × 24 μm and the resolving power was 45 000.

Finally, twelve echelle spectra were obtained in February 2000 with the 1.2m Euler Swiss telescope at La Silla, equipped with the Coralie spectrograph and a 2k × 2k CCD with pixel size 15 μm × 15 μm. The Coralie instrument is an improved version of the Elodie spectrograph (Baranne et al. 1996). These observations covered the spectral range 3875 - 6800 Å with a resolving power of 50 000. The integration times varied between 30 and 45 minutes and the typical S/N ratio at 5000 Å was 120 - 150.

The CAT data were reduced in a standard way with the MIDAS software developed at ESO. The spectra were normalized by fitting a low order polynomial to the continuum. The FEROS spectra were reduced using the appropriate context of the MIDAS environment together with several dedicated routines kindly provided by Dr. O. Stahl. The extracted FEROS spectra were rectified by fitting a polynomial of degree 4 or 5 to the continuum over a range of a few hundred Å at once.

The CTIO data were reduced using the IRAF[1] package, following the recommendations of the BME User's Manual. We used the smoothed projector flat field exposures as a first guess of the continuum, and the spectra were finally normalized using a low-order polynomial.

The Coralie data were reduced at the telescope, using the INTER-TACOS (INTERpreter for the Treatment, the Analysis and the COrrelation of Spectra) software developed by D. Queloz and L. Weber at the Geneva Observatory (Baranne et al. 1996). Next, the normalisation was done by dividing by the blaze fits and finally by fitting a polynomial to the continuum.

[1] IRAF is distributed by the National Optical Astronomy Observatories.

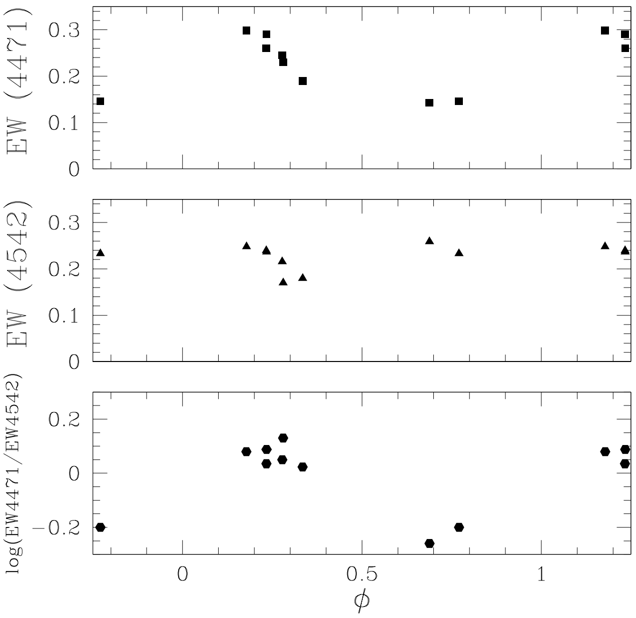

Fig. 2. Variations of the equivalent width of the He I λ 4471 and He II λ 4542 lines and of the log(W') criterion for the primary star as a function of orbital phase.

Whenever several exposures were available for the same night, we averaged them to increase the S/N ratio. Some preliminary results based on our data were already presented by Nazé et al. (2000).

3. The spectrum of HD 149404

A FEROS spectrum of HD 149404 is shown in Fig. 1. Besides the lines of the upper Balmer series (above Hγ), the spectrum reveals many typical O-star absorption lines of He I, He II, N III, Si III, Si IV, C IV and O III. The less massive star exhibits strong N III absorptions whereas N III is seen as a weak absorption or emission (N III $\lambda\lambda$ 4634-41) in the primary's spectrum. The spectrum reveals also a number of diffuse interstellar bands (DIBs), as well as interstellar absorptions due to Na I, Ca II, CH and CH$^+$. However, the most remarkable feature of HD 149404 is the important number of emission lines in its spectrum: Hα, Hβ, He II λ 4686, C III λ 5696, as well as several N II and Si IV lines. We will come back to some of these features in the next sections. Throughout this paper we will refer to the more massive star as the primary.

3.1. Spectral types

Only the least blended spectra are suitable for the spectral classification. Following Conti & Alschuler (1971), Conti & Frost (1977) and Mathys (1988, 1989), we adopt the $\log W' = \log\left(EW(4471)/EW(4542)\right)$ classification criteria. We caution that the equivalent width (EW) of the He II λ 4542 line of the individual components is rather difficult to measure in the case of HD 149404 because of the severe blending.

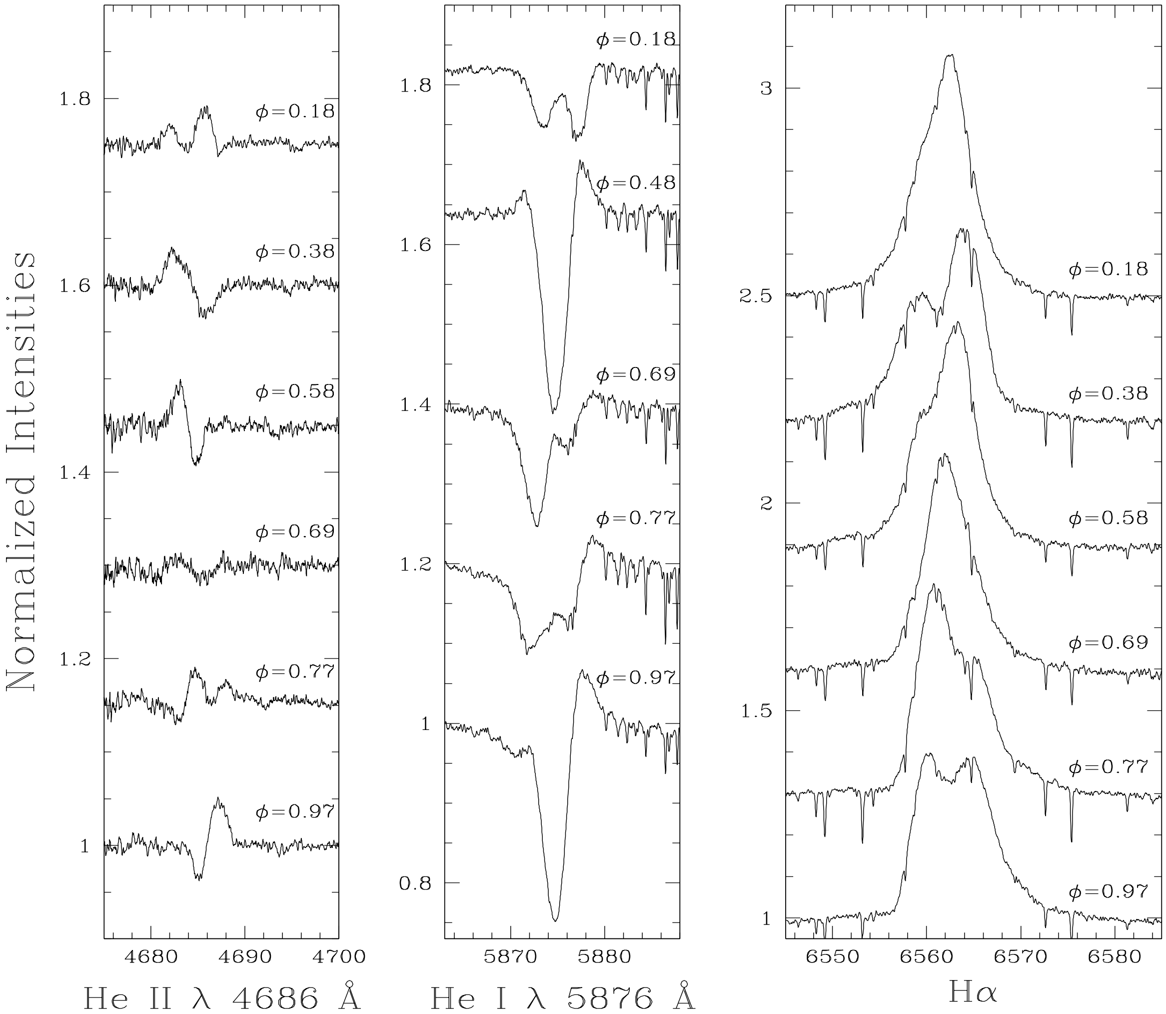

Fig. 3. Variation of the He II $\lambda\,4686$, He I $\lambda\,5876$ and Hα lines with phase.

For the secondary, we find $\log W'$ between 0.51 and 0.83, corresponding to a spectral type O9.7 (using the Mathys criteria). The O9.7 classification is also supported by the fact that the He II $\lambda\,4542$ and Si III $\lambda\,4552$ absorptions have about the same strength (Walborn & Fitzpatrick 1990).
For the primary, we obtain $\log W'$ between -0.26 and 0.13. More specifically, we find an O6.5 spectral type for orbital phases near 0.75, i.e. when the primary is moving towards us (see Fig. 2), and an O7.5 type half a period later. In fact, Fig. 2 indicates that the orbital variation of $\log W'$ is essentially due to the variation of the equivalent width of the He I $\lambda\,4471$ line. It is interesting to note that the He I $\lambda\,4471$ absorption of the secondary displays the opposite behaviour[2], i.e. it appears stronger around $\phi = 0.75$ and weaker near $\phi = 0.25$ (Nazé et al. 2000). The behaviour of both absorption components at He I $\lambda\,4471$ could therefore at least partially reflect the blending with a weak, slightly red-shifted emission component that does not follow the orbital motion of neither star. Such an emission feature is indeed seen in the He I $\lambda\,5876$ line (see Fig. 3) and we actually detect a weak emission on some of the He I $\lambda\,4471$ spectra taken near conjunction. At phases near 0.75, the emission is blended with the primary's absorption, hence reducing its equivalent width. The reverse situation occurs half a cycle later, when the secondary's absorption is blended with the emission. As the primary's EW is most probably less affected by the emission feature around $\phi = 0.25$, we adopt the O7.5 classification for this star (see also Nazé et al. 2000).

For the luminosity classification, we rely on the $\log W'' = \log\,(EW(\mathrm{Si\,IV}\,\lambda\,4089)/EW(\mathrm{He\,I}\,\lambda\,4143))$ criterion introduced by Conti & Alschuler (1971). This turned out to be even more difficult than the spectral classification. In fact, He I $\lambda\,4143$ could be deblended on a few spectra only and we could only set an upper limit of $\leq\ 0.07\,\text{Å}$ on the EW of the primary's He I $\lambda\,4143$ line. For the secondary, we find $\log W''$

[2] We caution however that the variation of the $\log W'$ criterion of the secondary results also from variations of the EW of the He II $\lambda\,4542$ line that are more pronounced than for the primary.

between 0.36 and 0.65 corresponding to a supergiant classification. In the same way, our upper limit on the primary's EW(He I $\lambda\,4143$) yields $\log W'' \geq 0.4$ (at all orbital phases), also corresponding to luminosity class I. We caution that a similar effect as for the He I $\lambda\,4471$ line could alter the EWs of the He I $\lambda\,4143$ lines, although we do not expect this effect to significantly affect our conclusions.
On the other hand, He II $\lambda\,4686$ could be in absorption in the spectrum of both stars (see below), an unlikely feature for luminosity class I stars, especially for Ia stars (Walborn 1971). Finally, the N III $\lambda\lambda\,4634$-41 emission lines appear to follow more or less the motion of the primary. Therefore we add an (f) tag to the spectral classification of the primary.

3.2. Interstellar lines

We have measured the radial velocities (RVs) of the most prominent interstellar lines (Table 1). Both Ca II lines exhibit a blueshifted much fainter component which is only visible on the FEROS spectra.
We emphasize the very good night-to-night stability of the FEROS and Coralie spectrographs as revealed by the small 1-σ dispersions of the RVs in Table 1. There is a slight difference of the order of $0.5\,\mathrm{km\,s^{-1}}$ between the RVs derived from the FEROS and the Coralie data. Moreover, we notice that there is a slight RV-difference between the Ca II and Na I lines. Stickland & Koch (1996) adopted a radial velocity of $-7.5\,\mathrm{km\,s^{-1}}$ for the interstellar features in their *IUE* spectra, which is consistent with our results for the Na I lines.

Table 1. Radial velocities (in $\mathrm{km\,s^{-1}}$) of the most prominent interstellar lines in the spectrum of HD 149404. The quoted uncertainties correspond to the 1-σ dispersion of the RVs measured during the same observing run.

Line	FEROS 1999	Coralie	FEROS 2000
Ca II $\lambda\,3933$	-3.9 ± 0.2	-4.5 ± 0.3	-2.7 ± 0.1
Ca II $\lambda\,3968$	-3.8 ± 0.3	-5.3 ± 0.5	-3.8 ± 0.1
CH^+ $\lambda\,3958$	-2.4 ± 0.6	-3.6 ± 2.9	-2.3 ± 0.8
CH^+ $\lambda\,4233$	-1.6 ± 0.6	-2.7 ± 0.4	-1.9 ± 0.4
CH $\lambda\,4300$	-0.4 ± 0.2	-1.0 ± 0.3	-0.4 ± 0.4
Na I $\lambda\,5890$	-7.8 ± 0.3	-8.4 ± 0.4	-8.2 ± 0.0
Na I $\lambda\,5896$	-7.9 ± 0.3	-8.2 ± 0.3	-7.9 ± 0.0

4. Orbital Solution

4.1. Radial Velocity Determination

Since He I $\lambda\,4471$ is the most extensively covered absorption line in our data set and since it is also usually the least blended one, we decided to use the RVs of this line to determine a new orbital solution. Other lines are either weak (e.g. He II $\lambda\,4542$), blended with other weaker absorptions (He II $\lambda\,4200$ blended with N III $\lambda\,4196$) or affected by a rather strong emission component (He I $\lambda\,5876$). These features are thus not well suited to measure the RVs of the binary components.
We notice that the intensities of the absorption lines (including He I $\lambda\,4471$, see Fig. 2 and Nazé et al. 2000) change with phase. This phenomenon is not unexpected since HD 149404 is known to display variations of the line strength in the UV that could be related to the so-called 'Struve-Sahade effect' (Stickland 1997).
The radial velocities were determined by fitting two gaussians whenever it was possible to do so. However, the lines remain heavily blended over the main part of the orbit and even around quadrature the lines are not completely separated. Therefore, two different techniques were tested to determine the radial velocities when gaussian fitting turned out to be impossible. In both cases we use a template line profile built from the spectra at maximum separation.

(1) When the lines are partially blended, the 'outer' wing of the strongest line is rather unaffected by the other line. Fitting the corresponding wing of the template spectrum to the observed profile yields the position of the strongest line. Next, the template profile of the strongest line is shifted to the correct position and subtracted from the observed spectrum. The position of the weaker line is finally obtained by fitting a gaussian to the residuals.
(2) Alternatively we have attempted a simultaneous fit of the positions of the lines of both components. To this aim we have shifted both templates independently and simultaneously until we found a best fit to the observed profile.

The resulting radial velocities are presented in Table 2.

Given the difficulties due to the severe blending of the lines, we also used another method developed at the Geneva observatory to determine the radial velocities. The velocities are obtained by cross-correlation of the FEROS and Coralie spectra with a mask built from a synthetic spectrum. This method is well known for less massive stars, but this is the first attempt to extend it to the optical spectra of O-type stars. A synthetic O-star spectrum in the 3875-6820 Å spectral domain was generated using the SYNSPEC (Hubeny et al. 1994) code with the model atmospheres interpolated from the Kurucz ATLAS9 (1994) grid. The Vienna Atomic Line Database was used to create a line list for the spectrum synthesis (Kupka et al. 1999). The spectrum synthesis programme uses an LTE-model which is certainly not appropriate to determine the properties of O-stars, but should be sufficient for the radial velocity determinations. Many tests were conducted and eventually, a synthetic spectrum with $T_{\rm eff} = 42500$ K was adopted because it provided the most narrow cross-correlation peak. Blended lines as well as emission lines or lines that occur in the synthetic spectrum but are absent from the actual spectrum were removed from the mask. Therefore, the final mask no longer corresponds to a single $T_{\rm eff}$ but should be valid over a rather broad temperature range from about 35000 to 42500 K. The radial velocities were finally obtained from the cross-correlation function by fitting two gaussians. The results are presented in the last two columns of Table 2.

Table 2. Barycentric radial velocities obtained for He I λ 4471 and by a correlation with a synthetic mask. The dates of the observations are given in the format HJD–2450000 and the orbital phases are those corresponding to the circular orbital solution derived from the cross-correlation RVs (see Table 3). The method used to derive the RVs of the He I λ 4471 line is specified in the sixth column: d(nbr of gaussians) = gaussian fit, c1 (c2) = 1st (2nd) technique (see text), m = mean of techniques listed in brackets.

Instr.	Date	ϕ	He I λ 4471			cross-correlation	
			RV_1 km s^{-1}	RV_2 km s^{-1}	Method	RV_1 km s^{-1}	RV_2 km s^{-1}
LC	622.588	0.23	−107.0	71.7	d(2)		
LC	623.595	0.34	−107.1	35.5	m(c1,c2)		
LC	624.552	0.43	−86.9	−14.2	m(c1,c2)		
LC	625.593	0.54	−58.2	−58.2	d(1)		
LC	626.556	0.64	−12.3	−109.4	c1		
VLC	925.944	0.14	−103.4	26.8	m(d(2),c1)		
VLC	926.944	0.24	−124.2	47.6	d(2)		
VLC	930.884	0.65	0.2	−136.9	m(d(2),c1)		
VLC	932.946	0.86	−21.2	−124.6	m(d(2),c1)		
VLC	937.914	0.36	−111.9	13.7	c1		
VLC	995.635	0.24	−116.6	72.5	d(2)		
VLC	996.565	0.34	−96.9	31.3	m(c1,c2)		
VLC	997.581	0.44	−66.3	4.1	m(c1,c2)		
VLC	998.572	0.54	−73.9	−73.9	d(1)		
VLC	999.572	0.64	−48.5	−147.4	m(c1,c2)		
VLC	1000.544	0.74	36.7	−160.6	d(2)		
FER.	1299.800	0.23	−117.8	52.9	d(2)	−108.0	55.5
FER.	1300.793	0.34	−118.8	43.5	d(2)	−109.0	49.7
FER.	1301.797	0.44	−79.6	−23.6	c2	−67.1	3.0
FER.	1302.788	0.54	−67.5	−67.5	d(1)	−39.2	−70.5
FER.	1304.796	0.74	28.5	−127.6	d(2)	12.4	−138.5
FER.	1323.741	0.67	43.8	−119.7	d(2)	15.4	−124.0
FER.	1327.766	0.08	−77.6	4.6	c2	−75.0	2.5
BME	1328.700	0.18	−135.5	−0.5	c2		
BME	1329.705	0.28	−131.3	46.0	d(2)		
BME	1330.707	0.38	−92.9	0.6	c2		
BME	1331.717	0.49	−52.5	−52.5	c2		
BME	1332.728	0.59	−32.8	−120.5	c2		
COR.	1578.866	0.67	38.8	−115.1	d(2)	6.8	−123.1
COR.	1579.879	0.77	38.0	−139.7	d(2)	18.8	−146.6
COR.	1580.872	0.87	−45.5	−122.1	c2	−9.6	−111.9
COR.	1581.864	0.97	−58.8	−58.8	d(1)	−34.2	−64.0
COR.	1582.869	0.08	−70.5	11.2	d(2)	−80.6	−3.7
COR.	1583.877	0.18	−92.8	63.5	d(2)	−98.0	54.7
COR.	1584.857	0.28	−101.0	65.9	d(2)	−99.7	58.1
COR.	1585.845	0.38	−84.4	8.9	d(2)	−85.9	8.2
COR.	1586.870	0.48	−46.6	−46.6	d(2)	−65.0	−30.9
COR.	1587.861	0.58	−48.2	−104.7	c2	−10.0	−89.8
COR.	1588.886	0.69	31.8	−133.8	d(2)	8.1	−132.9
COR.	1590.886	0.89	−49.8	−108.3	c2	−9.1	−98.5
FER.	1668.892	0.84	−44.2	−150.0	c2	−4.4	−127.2
FER.	1669.769	0.93	−73.5	−73.5	d(1)	−18.1	−82.2
FER.	1670.770	0.03	−46.1	−46.1	d(1)	−61.0	−15.0
FER.	1671.775	0.13	−95.3	27.8	d(2)	−85.5	27.9
FER.	1672.766	0.23	−104.6	67.4	d(2)	−102.5	64.8
FER.	1673.895	0.35	−106.7	18.8	d(2)	−89.6	33.7

4.2. Period determination

We used the generalized Fourier spectrogramme technique of Heck et al. (1985, hereafter HMM, see their Eq. 1) and the methods of Renson (1978) and Lafler & Kinman (1965, hereafter LK) to determine an improved value of the orbital period. To this aim, we applied the period search techniques to the time series of the $\mathrm{RV}_1 - \mathrm{RV}_2$ radial velocity differences as determined from the He I λ 4471 line in our data. To improve the accuracy of the result, we included also the data of Stickland & Koch (1996). The HMM method yields an orbital period of 9.81475 days (in agreement with the results of the Renson method) whilst the LK method yields 9.81431 days.

Table 3. Orbital solutions adopting a period of $P = 9.81475$ days and assuming $e = 0.0$. T_0 corresponds to the conjunction with the secondary in front. The quoted errors correspond to 1 σ uncertainties.

	He I λ 4471		cross-correlation	
	Prim.	Second.	Prim.	Second.
T_0(HJD–2450000)	1680.188 ± 0.531		1680.279 ± 0.174	
γ (km s^{-1})	-54.0 ± 5.2	-46.4 ± 11.5	-46.6 ± 1.7	-41.6 ± 3.5
K (km s^{-1})	62.8 ± 6.0	99.1 ± 9.0	59.7 ± 2.0	98.7 ± 3.2
$a \sin i$ (R$_\odot$)	12.2 ± 1.2	19.2 ± 1.9	11.6 ± 0.4	19.1 ± 0.6
$m \sin^3 i$ (M$_\odot$)	2.64 ± 0.66	1.68 ± 0.42	2.52 ± 0.21	1.52 ± 0.13
$q = m_2/m_1$	0.634 ± 0.085		0.605 ± 0.027	
$R_{\rm RL}/(a_1 + a_2)$	0.42 ± 0.01	0.34 ± 0.01	0.42 ± 0.01	0.34 ± 0.01
$R_{\rm RL} \sin i$ (R$_\odot$)	13.2	10.7	13.0	10.3
$rms\,(O - C)$ (km s^{-1})	18.3		6.1	

The estimation of the error on a period is not a straightforward problem. A secure upper limit on the error can be estimated from the width of the peak (which regardless of the method is of the order $1/\Delta T$ where ΔT is the total time spanned by the data set) i.e. 0.014 day in the present case. Empirically, the error is usually a substantial fraction of it. Under the hypothesis that the data are well distributed over ΔT and that the sampling does not suffer from any particular problem, we can use Eq. 20 of Lucy & Sweeney (1971) to compute a formal error. In the present case this yields $\sigma_P = 0.00084$ day. The three methods hereabove yield values of the period that overlap within the errors and in the following we will adopt the period obtained with the HMM technique.

4.3. Orbital elements

We used our radial velocity measurements to determine a new orbital solution. As a first step, we considered the possibility of an eccentric solution. The RVs determined by cross-correlation of our echelle spectra with a mask yield a very small eccentricity of $e = 0.02 \pm 0.02$. We notice that the RVs of the He I λ 4471 line alone yield a larger value of $e = 0.20 \pm 0.05$, but this result is most probably due to the systematic deviation of the He I λ 4471 RVs at certain orbital phases with respect to the RVs derived by cross-correlation. In the following, we will focus on the non-eccentric solutions. The orbital elements determined using the various datasets are listed in Table 3 and the curves shown in Figs. 4 and 5.

A simple inspection of the solutions listed in Table 3 shows that most of the orbital elements overlap within their errors. The errors on the cross-correlation solution are however much smaller and the data points show little scatter around the best fit solution. This illustrates the power of the mask cross-correlation technique to handle the orbital solutions of heavily blended early-type binaries and, in the following, we will use the orbital elements determined from this solution. The orbital phases used throughout this paper refer to the ephemerides from this latter solution.
The RVs determined for the He I λ 4471 line are usually in rough agreement with those determined by mask cross-correlation if we account for the slight difference in the γ velocities. A major disagreement is apparent around $\phi \sim 0.75$ for the RVs of the primary star that cluster systematically some 40 km s^{-1} above the best fit curve (Fig. 4). It is interesting to note that the most discrepant He I λ 4471 RVs occur precisely in the range of orbital phases when the primary's lines display a reduced EW. The discrepant RVs of the primary near $\phi \sim 0.75$ lead to a somewhat larger mass ratio inferred from the RVs of the He I λ 4471 line than from the cross-correlation RVs. In this context, we note that an orbital solution derived from the RVs of the He II λ 5412 line yields a mass ratio of 0.619 (Nazé et al. 2000), in better agreement with the value obtained from the cross-correlation method.

Our orbital solutions yield apparent systemic velocities for the two components that are somewhat different with the primary showing the more negative γ. This could indicate that the primary's wind is slightly stronger than that of the secondary. However, the effect is much smaller for HD 149404 than for some other evolved early-type binaries (e.g. Rauw et al. 1999, 2000b).

Table 4 provides an overview of the orbital solutions of HD 149404 available in the literature. We notice that the mass ratio determined from our solution is intermediary between the values proposed by Massey & Conti (1979) and by Stickland & Koch (1996). Several authors argue that the actual mass ratio might be close to unity. In fact, Massey & Conti (1979) suggested a value of $q \sim 1$ based on the RVs of the N III $\lambda\lambda$ 4634-41 emission lines which they attributed to the primary star. Though it has been shown that the N III emissions might actually form in the photosphere of Of-type stars (Mihalas & Hummer 1973), our observations of HD 149404 reveal a rather complex behaviour of these lines that is not consistent with a purely photospheric origin (see below). A mass ratio near unity was also suggested by Hutchings & van Heteren (1981) based on a preliminary analysis of four IUE spectra and by Penny et al. (1996) from a comparison of the location of the components of HD 149404 in the H-R diagram with theoretical evolutionary tracks of single stars. It is worth mentioning that all the prominent absorption lines in the spectrum of HD 149404 (He II λ 4542, He I λ 4713, He I λ 4921, N III $\lambda\lambda$ 4510-24, ...) yield a mass ratio in agreement with our orbital solution.

Table 4. Orbital solutions from the literature. T_0 corresponds to the conjunction with the less massive star in front.

	Massey & Conti		Stickland & Koch	
	Prim.	Second.	Prim.	Second.
P(days)	9.813		9.81452	
T_0(HJD-2440000)	2503.607		4446.849	
e	0 (adopted)		0 (adopted)	
$\gamma(\mathrm{km\,s^{-1}})$	−28.0	−37.0	−60.0	−52.5
$K(\mathrm{km\,s^{-1}})$	60.0	101.0	64.3	98.1
$a\,\sin i\,(\mathrm{R}_\odot)$	11.60	19.63	12.47	19.04
$m\,\sin^3 i\,(\mathrm{M}_\odot)$	2.7	1.6	2.64	1.73
$q = m_2/m_1$	0.595		0.655	
Spectral types	O7 III(f)	O8.5 I		

Finally, we note that including the Stickland & Koch (1996) data in our orbital solution yields orbital elements very similar to those found from our data alone.

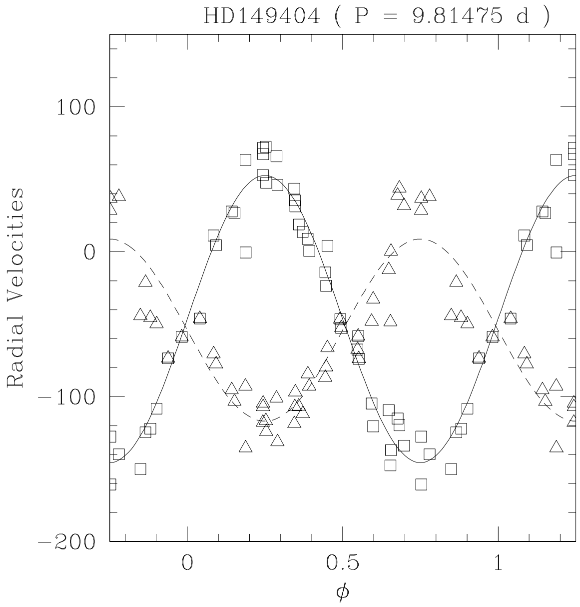

Fig. 4. Radial velocity curve of the He I λ 4471 line in the spectrum of HD 149404 as a function of the orbital phase and assuming $e = 0.0$ (see Table 3). The triangles correspond to the primary's RVs while the squares indicate the RVs of the secondary.

4.4. Inclination

Massey & Conti (1979) report a photometric study of HD 149404 by Dr. N. Morrison that revealed some variability at a rather low level (0.03 mag). The lightcurve could probably be explained by ellipsoidal variations but there are not enough data points to draw any firm conclusion (Morrison 2000).
Luna (1988) obtained polarimetric observations of HD 149404 that yield only an upper limit of 50° on the orbital inclination.
Vanbeveren & de Loore (1980) propose an inclination of 28° based on the orbital solution of Massey & Conti (1979) and on

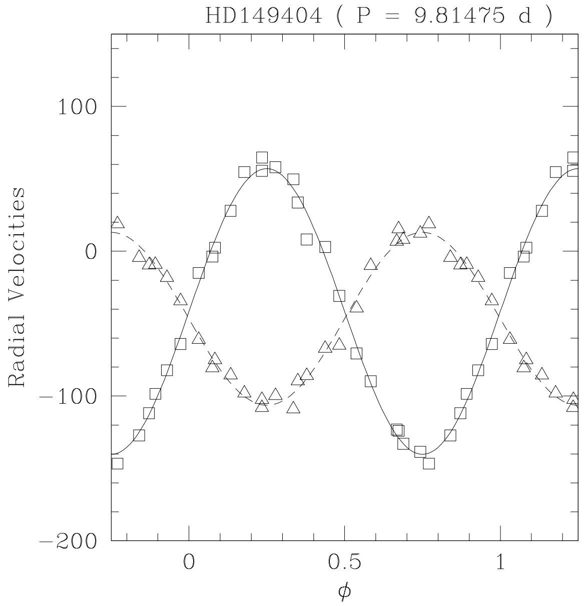

Fig. 5. Radial velocity curve determined by the mask cross-correlation method as a function of the orbital phase (assuming a circular orbit, see Table 3).

a comparison of the primary parameters with typical masses of O7 stars. Penny et al. (1996) derived an upper limit of 31° from the condition that neither of the two stars should fill its Roche lobe, and a lower limit of 15° by setting an upper limit of 150 $\mathrm{M}_\odot$ on the primary's mass.
Comparing our minimum masses from Table 3 with 'typical' masses of O9.7 I and O7.5 I supergiants (e.g. Howarth & Prinja 1989), we find an inclination of 20.3° for the primary and 21.0° for the secondary. Adopting 21° as a 'realistic' estimate, the Roche lobe radii are equal to 36 $\mathrm{R}_\odot$ and 29 $\mathrm{R}_\odot$ for the primary and secondary respectively. According to Howarth & Prinja (1989), the typical radii of O9.7 I and O7.5 I supergiants are 21 and 26 $\mathrm{R}_\odot$ respectively. With that inclination, it seems *a priori* unlikely that any of the two components fills its Roche lobe. However, we will come back to this point in Sect. 7.1.

5. Spectroscopic luminosity ratio

In principle, a rough estimate of the visible luminosity ratio of the binary components can be inferred from the ratio of the equivalent widths of absorption lines in the primary's and secondary's spectra (e.g. Rauw et al. 2000a):

$$\frac{I_{\rm prim}}{I_{\rm sec}} = \left(\frac{EW_{\rm prim}}{EW_{\rm sec}}\right)_{\rm obs} \times \left(\frac{EW_{\rm O9.5I}}{EW_{\rm O7.5I}}\right)_{\rm typ}$$

where $\left(\frac{EW_{\rm O9.5I}}{EW_{\rm O7.5I}}\right)_{\rm typ}$ stands for the ratio of the EWs of the lines as observed in typical single O9.5 I (as a best substitute for O9.7 I) and O7.5 I stars. We measured the EW ratios of the He I $\lambda\lambda$ 4026, 4471, He II λ 4542 and Si IV $\lambda\lambda$ 4089, 4116 absorption lines (see Table 5). The typical EW ratios were derived from the compilation of O-star equivalent widths published by Conti & Alschuler (1971) and Conti (1973, 1974).

In the case of HD 149404, the main limitation of the method stems from the strong orbital variability of the line strength (see Table 5). For instance, the strength of the primary's Si IV lines around $\phi \sim 0.75$ is reduced by a factor 2 with respect to $\phi \sim 0.25$, while the strength of the secondary's Si IV lines simultaneously increases by about a factor 1.3. An easy way to account for the fading of the primary's lines around $\phi \sim 0.75$ and the simultaneous strengthening of the secondary's absorptions would be to assume that one of the two stars was brighter on the front side than on the rear. However, since the amplitude of the photometric variations is only a few percent, it seems rather unlikely that the observed EW variations reflect actual variations of the brightness of one of the binary components, otherwise a larger amplitude of the light curve would be expected.

We notice that the total EW (primary + secondary) varies by only about 5% for the absorptions considered here. On the other side, we know that the He I lines are most probably affected by an emission component and the EW of the primary's He I lines are reduced around $\phi \sim 0.75$ (see Fig. 2). Therefore, blending with a most probably slightly red-shifted emission component not associated with either of the two stars could be an explanation for the observed variations.

Similar difficulties are encountered in the UV. Howarth et al. (1997) derived a mean raw UV magnitude difference of 0.8 with the secondary being the brighter component. Correcting this magnitude difference for the different spectral types, we obtain a UV luminosity ratio (primary/secondary) of roughly 0.6. Stickland & Koch (1996) reported a luminosity ratio of about 1.0 when the primary is moving towards us (our phase 0.25) and about 0.5 when it is moving away (our phase 0.75).

Using the results for the He II and Si IV lines from Table 5, we calculate a mean luminosity ratio of about 1.4 ± 0.4 near $\phi \sim 0.25$ and 0.5 ± 0.1 near $\phi \sim 0.75$.

Assuming that the observed EWs are indeed reduced by a red-shifted emission component, we can derive the 'actual' spectroscopic luminosity ratio using the mean EWs of each star's line when the star is moving towards us. In this way, we find an average ratio of $\overline{\mathrm{I}}_{\rm prim}\,(0.25)/\overline{\mathrm{I}}_{\rm sec}\,(0.75) = 0.90 \pm 0.16$ (see Table 5).

Alternatively, the absorption enhancement seen when the lines are blueshifted could be due to material from a wind interaction region that would be swept up by the star during its orbital motion. In this case, the front sides of the stars would display abnormal line strengths and the actual luminosity ratio would best be derived from the mean EWs of the lines observed when the stars are moving away from us. This assumption yields an average ratio of $\overline{\mathrm{I}}_{\rm prim}\,(0.75)/\overline{\mathrm{I}}_{\rm sec}\,(0.25) = 0.75 \pm 0.23$ (see Table 5). This result overlaps within the errors with the value of the $\overline{\mathrm{I}}_{\rm prim}\,(0.25)/\overline{\mathrm{I}}_{\rm sec}\,(0.75)$ ratio. In this second scenario, each star would have to sweep up about the same amount of material in order to explain the roughly constant total EWs of the lines. Therefore, it seems more likely that the variations of the apparent luminosity ratio are rather due to an unresolved emission component and in the following we shall thus adopt a spectroscopic luminosity ratio of 0.90 ± 0.16.

6. Emission lines

The spectrum of HD 149404 exhibits many emission lines some of which display strong orbital variability.

- The unidentified $\lambda\lambda$ 4486, 4504 emission lines appear to be associated with the secondary star as shown by Nazé et al. (2000). These emission lines are a common feature in the spectra of the most luminous stars between spectral type O7 and O9.5 (Conti 1973, Walborn & Fitzpatrick 1990).
- N III $\lambda\lambda$ 4634-41: the bulk of the emission seems to follow the primary whilst the lines are observed in absorption in the secondary's spectrum. The RV behaviour of the N III emissions itself is however rather complex and the lines are quite broad and display strong profile variability probably indicating that these lines are not purely stellar features.
- He II λ 4686 (see Fig. 3) consists of a mixture of emission and absorption lines and the line morphology displays strong phase-locked variations. The emissions do not follow the orbital motion of the stars. Instead, both stars exhibit this line in weak absorption though the visibility of these absorption features varies strongly with phase and the absorption lines vanish near phases 0.2 and 0.7.
- A similar situation is observed for the Hβ line. As for He II λ 4686, the stellar Hβ lines are again in (rather weak) absorption and the composite line profile suffers strong variability with an emission feature that does not follow the motion of either star. We caution that the Hβ profile is blended with the N III $\lambda\lambda$ 4858-67 absorption lines and this blend probably affects the radial velocity measurements of the Hβ emission components.
- Our echelle spectra reveal N II emission features at $\lambda\lambda$ 5001-12, 5667, 5932, 5940-42, 5952, 6482 and 6611, that are associated with the O9.7 secondary. Walborn (1980) reported weak N II $\lambda\lambda$ 5940-42, 6482 emission in the ON9.7 Iae star HD 105056. The presence of the N II emissions and the strength of the N III absorption lines in the spectrum of the secondary of HD 149404 could therefore indicate that nitrogen is enhanced in the atmosphere of this star. Further support for an ON classification of the secondary comes from the relative weakness of the C III $\lambda\lambda$ 4647-50 absorption compared to the intensity of this line in 'normal' O9.7 supergiants (see Walborn & Fitzpatrick 1990).
- The C III λ 5696 emission is probably formed by two independent features. The strongest component follows the orbital motion of the primary. This trend is confirmed by the variations of the line peak position (see Nazé et al. 2000). At some orbital phases (e.g. $\phi = 0.67$), a second emission peak appears with a velocity indicating that it is most probably associated with the secondary.
- In addition to the absorption lines, He I λ 5876 displays a variable emission which is particularly strong at phases near 0.0 and 0.5 (see Fig. 3). This emission is probably present in other He I lines too, maybe causing part of the intensity and EW variations.
- The strongest emission feature in the visible spectrum of HD 149404 is Hα (see Fig. 3). The line exhibits a double peaked structure at certain phases, more or less in quadra-

Table 5. Luminosity ratios (primary/secondary) derived for different lines at different orbital phases. Typical uncertainties on the observed EW ratios are less than 10%. The colons indicate those measurements that have larger uncertainties due to heavier blending. The last two columns list the luminosity ratios derived from the mean EWs measured when the components are moving towards us (column 7) or when they are moving away from us (column 8); see the text for further details.

HJD–2450000	1299.800	1584.857	1672.766	1304.796	1579.879		
ϕ	0.234	0.278	0.235	0.743	0.771	$\bar{\mathrm{I}}_{\mathrm{prim}}\,(0.25)/\bar{\mathrm{I}}_{\mathrm{sec}}\,(0.75)$	$\bar{\mathrm{I}}_{\mathrm{prim}}\,(0.75)/\bar{\mathrm{I}}_{\mathrm{sec}}\,(0.25)$
He I λ 4026	1.70	1.13	1.95	0.28	0.41	0.86	0.66
He I λ 4471	1.35	1.19	1.51	0.35	0.47	0.84	0.60
He II λ 4542	1.71	1.22:	1.95		1.15:	1.19	0.66
Si IV λ 4089	1.07	0.90	1.11	0.39	0.91:	0.83	0.61
Si IV λ 4116	1.40	1.25	1.57	0.54		0.80	1.21

ture with the orbital motion. Though the visibility of the emission peaks in the Hβ profile is hampered by the blending with the stellar absorption lines, they seem nevertheless to follow more or less the behaviour of the Hα peaks, pointing towards a similar origin. In Sect. 7.2, we will discuss the variability of the Hα emission line in terms of a wind interaction model.

To further analyse the emission features, we apply a so-called 'S-wave analysis' (see e.g. Richards et al. 1996). We adopt two axes centred on the center of mass of the binary; the x axis points towards the secondary star while the direction of the y axis is given by the orbital motion of the secondary. We measured the RVs of the peaks of the most prominent emission lines and fitted a sine-wave expression

$$v(\phi) = -v_x\,\cos(2\pi\phi) + v_y \sin(2\pi\phi) + v_z$$

to these points (see e.g. Rauw et al. 1999). The results are summarized in Table 6 and a projected Doppler map is presented in Fig. 6. We caution that the quality of the fit to the RVs of the N III $\lambda\lambda$ 4634-40 lines is rather poor, mainly because of the variable shape of these lines.

Table 6. Results of the S-wave analysis: Coralie observations are not included for the N III emissions.

	v_x	v_y	v_z
? λ 4486	−0.1	87.3	−39.1
? λ 4504	2.7	80.6	6.5
N III λ 4634	−9.6	−73.6	−36.9
N III λ 4641	−16.9	−105.8	−52.8
C III λ 5696	22.3	−62.6	−42.5
N II λ 5932	8.3	108.0	−81.7
N II λ 5942	16.3	109.7	−44.8
He II λ 4686	−128.6	−82.4	−99.7
He II λ 4686	80.6	−65.3	16.4
Hβ	−123.8	−153.2	−47.1
Hβ	136.7	57.0	−47.8
Hα	−119.2	−75.1	−44.4
Hα	106.2	24.0	−53.4

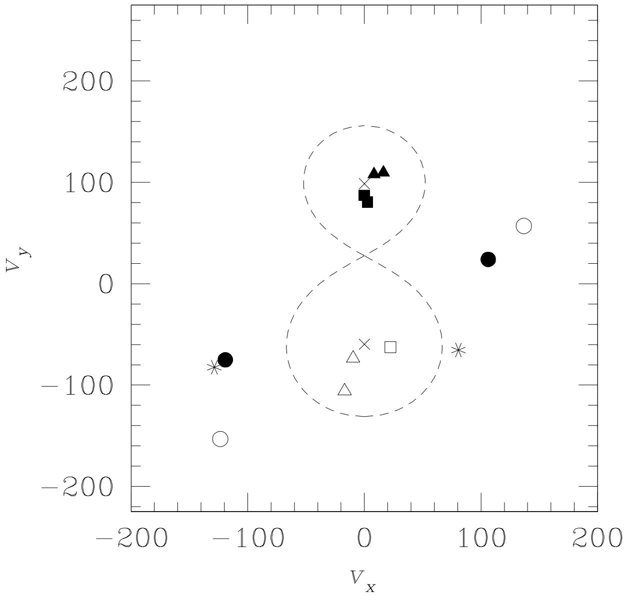

Fig. 6. Doppler map showing the results of our S-wave analysis projected on the (v_x, v_y) velocity plane. The crosses indicate the velocity of the center of mass of the binary components as derived from our orbital solution while the dashed line is the equivalent of the Roche lobe in velocity space. The different symbols stand for different emission lines: filled circles = Hα; open circles = Hβ; filled triangles = N II $\lambda\lambda$ 5932, 5942; open triangles = N III $\lambda\lambda$ 4634-41; filled squares = $\lambda\lambda$ 4486, 4504; open square = C III λ 5696 and stars = He II λ 4686.

The positions of the $\lambda\lambda$ 4486, 4504, C III λ 5696, N III $\lambda\lambda$ 4634-40 and N II $\lambda\lambda$ 5932, 5942 emission regions in velocity space indicate that the bulk of these emissions arises most probably within the atmospheres of the stars. On the other side, our analysis reveals that this is not the case for the Hα, Hβ and He II λ 4686 emissions. The latter lines exhibit a double peaked structure at orbital phases near conjunction and a single peak around quadrature. Assuming that the two peaks actually cross over, we have fitted their RVs with the above sine-wave expression. We caution here that only the Hα peaks are free from blends with absorption lines. The Hβ and He II λ 4686 lines are usually 'polluted' by absorption lines and the results for these lines should therefore be regarded only as trends roughly confirming the behaviour of the Hα peaks.

7. Discussion

7.1. The evolutionary status

Adopting the effective temperature calibration of Chlebowski & Garmany (1991), the spectral types we have derived yield $T_{\rm eff} = 35100 \pm 1000$ K and $T_{\rm eff} = 30500 \pm 400$ K for the primary and the secondary respectively. HD 149404 has an apparent V magnitude of 5.47 (Drilling 1991). Assuming that the star is a member of the Ara OB1a association ($DM = 10.7$, Humphreys 1978) and adopting a colour excess $E(B-V) = 0.68$ (Shull & Van Steenberg 1985) and a spectroscopic luminosity ratio of 0.90 ± 0.16 (see above), we derive $\log{(L_{\rm bol}^{\rm prim}/L_{\odot})} = 5.90 \pm 0.08$ and $\log{(L_{\rm bol}^{\rm sec}/L_{\odot})} = 5.78 \pm 0.08$ for the primary and secondary respectively. We caution that the error bars on the luminosities correspond only to the estimated error on the luminosity ratio and an uncertainty of half a spectral class for the bolometric correction. Our error bars account by no means for the (probably large) uncertainties on the distance of HD 149404.

The resulting locations of the components of HD 149404 in a H-R diagram are shown in Fig. 7 together with the theoretical evolutionary tracks of Schaller et al. (1992). We notice that the secondary star (i.e. the least massive star) seems to be the most evolved component though it lies on an evolutionary track of lower initial mass than the primary. This was already found by Penny et al. (1996), though these authors adopted different spectral types and hence derived different positions for the stars in the H-R diagram. As pointed out in Sect. 6, the strong N III absorptions and the N II emission lines seen in the secondary's spectrum could indicate that nitrogen is slightly enhanced in the atmosphere of this star, which would be a further indication that this star must be an evolved object. A possibility to account for the evolutionary status of the secondary would be to suppose that this star was initially the more massive component of the binary and has lost (or transferred) a considerable fraction of its mass through Roche lobe overflow in the past (see also Penny et al. 1996).

The temperatures and luminosities derived here correspond to radii of 24.3 and 28.1 $R_{\odot}$ for the primary and the secondary respectively. Therefore, the radius of the secondary star appears larger than we would expect from the 'typical' parameters listed by Howarth & Prinja (1989). Howarth et al. (1997) derived projected rotational velocities of $v_e \sin i = 91 \,{\rm km\,s^{-1}}$ and $100 \,{\rm km\,s^{-1}}$ for the O7.5 and the O9.7 component respectively. Assuming that the stars have the same angular rotational velocity (though the rotation needs not necessarily be synchronous with the orbital motion), we can derive the ratio of the stellar radii from the ratio of the projected rotational velocities. The value obtained in this way $R_{\rm prim}/R_{\rm sec} = 0.91$ is in very good agreement with the ratio of the radii derived above (0.86).

At this point, we need to return to the question of a current RLOF. In fact, the radius of the secondary star derived hereabove[3] (28.1 $R_{\odot}$) is only slightly smaller than the radius of its Roche lobe (29 $R_{\odot}$) for an inclination of 21°. Therefore a small error on the (poorly constrained) inclination has a large impact on our conclusion about the current configuration of HD 149404. Indeed, it could be that the secondary has just finished RLOF and is now settling down on a 'normal' evolutionary track corresponding to its current mass. Alternatively, the secondary could still be filling its critical volume and could be suffering an enhanced mass loss through the inner Lagrangian point.

[3] We caution that the actual value of $R_{\rm sec}$ depends on the adopted luminosity ratio between the two stars and the adopted distance towards HD 149404.

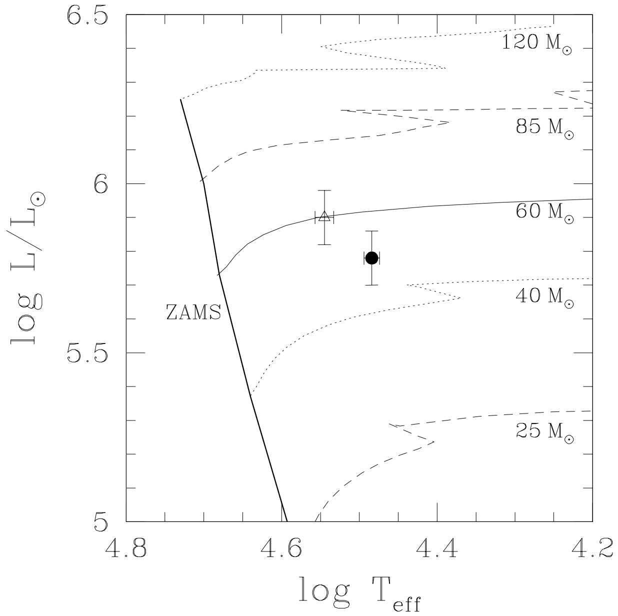

Fig. 7. Hertzsprung-Russell diagram of HD 149404. The open triangle stands for the primary star whilst the filled circle yields the position of the secondary star.

7.2. Towards a model for the wind interaction

In Sect. 6 we have shown that the Hα, Hβ and He II λ 4686 emission lines are not formed in the atmospheres of the stars but must be formed somewhere between the stars. Thaller (1998) suggested that the Hα emissions were coming from two focused stellar winds flowing towards a colliding wind interaction between the stars. Though the radius of the secondary star derived in Sect. 7.1 supports the possibility of an enhanced mass loss from the secondary focused towards the primary, it is not clear how the model suggested by Thaller (1998) could account for the RV behaviour found in Sect. 6. We favour an alternative model where the Hα emissions arise in the arms of a colliding wind shock region. Figure 8 displays a schematic view of such a wind interaction. As pointed out above, the secondary might actually be suffering a stronger mass loss than would be expected for a 'normal' O9.7 I star. Therefore, we assume that the two stars have roughly equally strong winds. The Coriolis force bends the arms of the shock region around both stars. In this model, the Hα emission forms through recombination in the hatched areas where the density is enhanced due to the shock (Fig. 8). The arrows indicate the

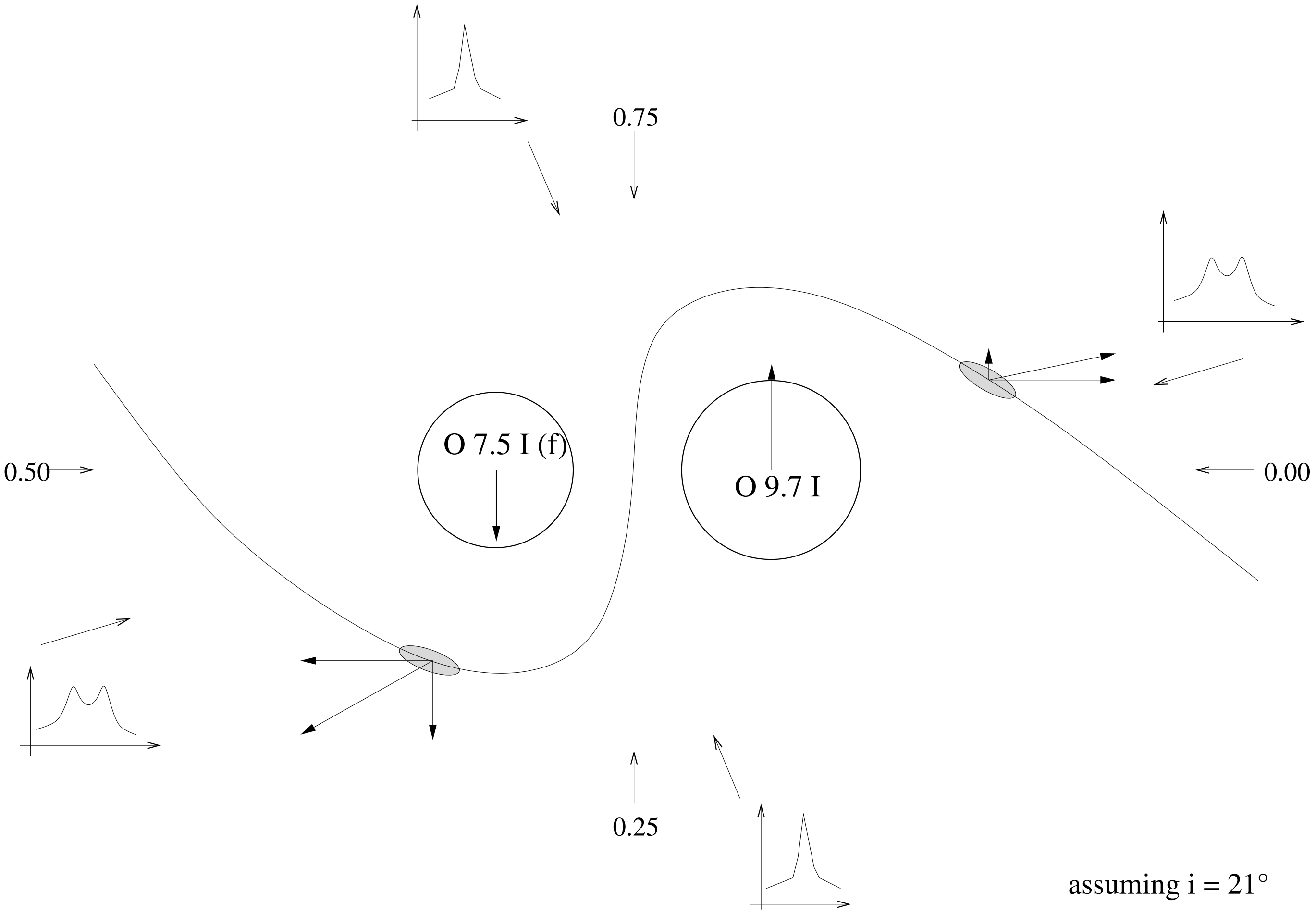

Fig. 8. Schematic view of the wind interaction in the HD 149404 system projected on the orbital plane. The changing morphology of the Hα line at some specific orbital phases is also sketched as a function of the line of sight. The relative dimensions of the orbit and the stars correspond to an inclination of $i = 21°$.

velocity components of the Hα emission regions as inferred from our S-wave analysis. The velocity components result from the combination of the orbital motion and the flow velocity of the plasma in the shock region.

In Fig. 8, the projections of the line of sight on the plane of the orbit are indicated for orbital phases near conjunction and quadrature. We see that this rather simple model can at least qualitatively account for the changing morphology and the RV behaviour of the Hα emission line in the spectrum of HD 149404.

We have analyzed *ROSAT* observations of HD 149404 to search for a signature of the wind interaction in the X-ray domain. HD 149404 was observed twice with *ROSAT*. A first exposure was obtained as part of the *ROSAT* All Sky Survey (Berghöfer et al. 1996). Another 3 ksec PSPC exposure was obtained on JD 2449056.813 ($\phi = 0.70$). We have retrieved this latter observation (rp201266) from the ARNIE database at Leicester University. The data were reduced using the XSELECT and XSPEC softwares. The background corrected PSPC count rate is $8.0\,10^{-2}$ cts s^{-1}. The PSPC spectrum is quite hard, as the ratio of the count rates in the ranges 0.5-2 keV and 0.1-0.5 keV is about 25. Despite the limited S/N ratio, we could fit an absorbed Raymond-Smith model (Raymond & Smith 1977) to the PSPC spectrum fixing the neutral hydrogen column density to its interstellar value $\mathrm{N_H^{ISM}} = 2.5\,10^{21}$ cm^{-2} (Shull & Van Steenberg 1985). The best fit yields an X-ray temperature of 0.84 ± 0.10 keV and a luminosity in the 0.1 - 2.0 keV energy range of $L_X = 1.6\,10^{32}$ erg s^{-1} corresponding to a ratio $L_X/L_{\rm bol}$ of $3.0\,10^{-8}$, slightly lower than for typical O stars. This result is in agreement with the value found by Berghöfer et al. (1996). Thus the snapshot *ROSAT* observations reveal no indication of a strong X-ray excess that could be attributed to a colliding wind emission. This is in line with the results of Chlebowski & Garmany (1991) who found no significant X-ray excess in those O-star binaries that are in a semi-detached or a contact configuration.

7.3. Summary and conclusions

We have used an extensive set of high resolution spectra to derive new orbital elements for the early-type binary HD 149404. We have shown that the mask cross-correlation technique developed at the Geneva observatory can be successfully applied to disentangle heavily blended lines in massive binaries. Our results allowed us to propose a new spectral classification for the components. We find that the primary is of spectral type O7.5 I(f), while the secondary is most likely an ON9.7 I supergiant. The secondary seems to be the most evolved component of the system and its current evolutionary status could best be explained if the system has undergone a Roche lobe overflow episode during the past. The secondary could actually still be rather close to filling its critical volume and this could lead to an enhanced mass loss of the secondary.

The behaviour of the emission lines in the spectrum of HD 149404 points towards a wind interaction between the two stars. We propose a simple model where some of the optical emission lines arise in a heavily bended shock region. It seems likely that HD 149404 is currently in a rather short-lived evolutionary stage where the wind interaction could be strongly affected by an enhanced mass loss of the secondary star. We caution, however, that this rather simple picture of the interaction could be seriously complicated if the secondary actually filled its critical volume. In this context, we emphasize that some of the crucial parameters of HD 149404 such as its distance and the orbital inclination remain poorly constrained. All future observations that could help to determine these parameters would be extremely useful to fully understand this system.

Acknowledgements. We are grateful to H. Sana for taking the May 2000 spectra and for his help in the reduction of the FEROS data, and to Dr. E. Jehin and G. Parmentier for taking some of the CAT + VLC observations. We also thank an anonymous referee for his helpful comments. We are greatly indebted to the Fonds National de la Recherche Scientifique for multiple support. This research is also largely supported by contract P4/05 “Pôle d’Attraction Interuniversitaire” (SSTC-Belgium) and through the PRODEX XMM-OM and Integral Projects. Part of this work has been supported by the Swiss National Found for the Scientific Research. The SIMBAD database has been consulted for the bibliography.

References

Baranne, A., Queloz, D., Mayor, M., et al. 1996, A&AS, 119, 373
Berghöfer, T.W., Schmitt, J.H.M.M., & Cassinelli, J.P. 1996, A&AS, 118, 481
Chlebowski, T., & Garmany, C.D. 1991, ApJ, 368, 241
Conti, P.S. 1973, ApJ, 179, 181
Conti, P.S. 1974, ApJ, 187, 539
Conti, P.S., & Alschuler, W.R. 1971, ApJ, 170, 325
Conti, P.S., & Frost, S.A. 1977, ApJ, 212, 728
Conti, P.S., Leep, E.M., & Lorre, J.J. 1977, ApJ, 214, 759
Drilling, J.S. 1991, ApJS, 76, 1033
Gies, D.R., Bagnuolo, W.G.Jr., & Penny, L.R. 1997, ApJ, 479, 408
Heck, A., Manfroid, J., & Mersch, G. 1985, A&AS, 59, 63
Howarth, I.D., & Prinja, R.K. 1989, ApJS, 69, 527
Howarth, I.D., Siebert, K.W., Hussain, G.A.J., & Prinja, R.K. 1997, MNRAS, 284, 265
Hubeny, I., Lanz, T., & Jeffery, C.S. 1994, TLUSTY and SYNSPEC: A User’s Guide, Newsletter on Analysis of Astronomical Spectra (Univ. of St. Andrews)
Humphreys, R.M. 1978, ApJS, 38, 309
Hutchings, J.B., & van Heteren, J. 1981, PASP, 93, 626
Kaufer, A., Stahl, O., Tubbesing, S., et al. 1999, The Messenger, 95, 8
Kupka, F., Piskunov, N., Ryabchikova, T.A., Stempels, H.C., & Weiss, W.W. 1999, A&AS, 138, 119
Kurucz, R.L. 1994, Solar abundance model atmospheres for 0, 1, 2, 4, 8 km s^{-1}, CD-ROM No. 19, Smith. Astroph. Obs.
Lafler, J., & Kinman, T.D. 1965, ApJS, 11, 216
Lucy, L.B., & Sweeney, M.A. 1971, AJ, 76, 544
Luna, H.G. 1988, A&AS, 74, 427
Massey, P., & Conti, P.S. 1979, in IAU Symp. 83, Mass Loss and Evolution of O-Type Stars, eds. P.S. Conti & C.W.H. de Loore, 271
Mathys, G. 1988, A&AS, 76, 427
Mathys, G. 1989, A&AS, 81, 237
Mihalas, D., & Hummer, D.G. 1973, ApJ, 179, 827
Morrison, N.D. 2000, private communication
Nazé, Y., Carrier, F., & Rauw, G. 2000, in Interacting Winds from Massive Stars, eds. A.F.J. Moffat & N. St.-Louis, ASP Conf. Series, in press
Penny, L.R., Gies, D.R., & Bagnuolo, W.G.Jr. 1996, in Proc. 33rd Liège Int. Astroph. Coll., Wolf-Rayet Stars in the Framework of Stellar Evolution, eds. J.-M. Vreux et al., 289
Rauw, G., Vreux, J.M., & Bohannan, B. 1999, ApJ, 517, 416
Rauw, G., Sana, H., Gosset, E., Vreux, J.-M., Jehin, E., & Parmentier, G. 2000a, A&A, 360, 1003
Rauw, G., Sana, H., Vreux, J.-M., Gosset, E., & Stevens, I.R. 2000b, in Interacting Winds from Massive Stars, eds. A.F.J. Moffat & N. St.-Louis, ASP Conf. Series, in press
Raymond, J.C., & Smith, B.W. 1977, ApJS, 35, 419
Renson, P. 1978, A&A, 63, 125
Richards, M.T., Jones, R.D., & Swain, M.A. 1996, ApJ, 459, 249
Schaller, G., Schaerer, D., Meynet, G., & Maeder, A., 1992, A&AS, 96, 269
Shull, J.M., & Van Steenberg, M.E., 1985, ApJ, 294, 599
Stickland, D.J., & Koch, R.H., 1996, The Observatory, 116, 145
Stickland, D.J. 1997, The Observatory, 117, 37
Thaller, M.L. 1997, ApJ, 487, 380
Thaller, M.L. 1998, in Proc. Boulder-Munich II Worksh., Properties of Hot, Luminous Stars, ed. I.D. Howarth, ASP Conf. Series, 131, 417
Vanbeveren, D., & de Loore, C. 1980, A&A, 86, 21
Walborn, N.R. 1971, ApJS, 23, 257
Walborn, N.R. 1972, AJ, 77, 312
Walborn, N.R. 1980, ApJS, 44, 535
Walborn, N.R., & Fitzpatrick, E.L. 1990, PASP, 102, 379
Wiggs, M.S., & Gies, D.R., 1993, ApJ, 407, 252